View metadata, citation and similar papers at core.ac.uk

brought to you by CORE

provided by Digitale Bibliothek Thüringen

ilmedia

TECHNISCHE UNIVERSITÄT ILMENAU

Becker, Tatiana; Stolbov, Oleg V.; Borin, Dmitry Yu.; Zimmermann, Klaus; Raikher, Yuriy L.:

Basic magnetic properties of magnetoactive elastomers of mixed content

Original published in:	Smart materials and structures. - Bristol : IOP Publ.. - 29 (2020), 7, art. 075034, 15 pp.
Original published:	2020-06-10
ISSN:	1361-665X
DOI:	10.1088/1361-665X/ab8fc9
[*Visited:*	2020-08-14]

This work is licensed under a Creative Commons Attribution 4.0 International license. To view a copy of this license, visit https://creativecommons.org/licenses/by/4.0/

TU Ilmenau | Universitätsbibliothek | ilmedia, 2020
http://www.tu-ilmenau.de/ilmedia

OPEN ACCESS
IOP Publishing
Smart Materials and Structures
Smart Mater. Struct. **29** (2020) 075034 (15pp)
https://doi.org/10.1088/1361-665X/ab8fc9

Basic magnetic properties of magnetoactive elastomers of mixed content

T I Becker[1], O V Stolbov[2,3], D Yu Borin[4], K Zimmermann[1] and Yu L Raikher[2,5]

[1] Technical Mechanics Group, Faculty of Mechanical Engineering, Technische Universität Ilmenau, 98684 Ilmenau, Germany
[2] Institute of Continuous Media Mechanics, Ural Branch of Russian Academy of Sciences, 614068 Perm, Russia
[3] Perm National Research Polytechnic University, 614990 Perm, Russia
[4] Institute of Mechatronic Engineering, Technische Universität Dresden, 01062 Dresden, Germany
[5] Institute of Natural Sciences and Mathematics, Ural Federal University, 620083 Ekaterinburg, Russia

E-mail: tatiana.becker@tu-ilmenau.de and yuriy.raikher@gmail.com

Received 27 January 2020, revised 27 March 2020
Accepted for publication 4 May 2020
Published 10 June 2020

Abstract

The results of theoretical and experimental investigations of the polymer composites that belong to a class of magnetoactive elastomers with mixed magnetic content (MAEs-MC) are presented. The fundamental distinction of such composites from ordinary magnetoactive elastomers is that the magnetic filler of MAEs-MC comprises both magnetically soft (MS) particles of size 3–5 μm and magnetically hard (MH) particles whose size is an order of magnitude greater. Since MH particles of the magnetic filler are mixed into a composition in a non-magnetised state, this can ensure preparation of samples with fairly homogeneous distribution of the filler. The 'initiation' process of a synthesised MAE-MC is done by its magnetisation in a strong magnetic field that imparts to the sample unique magnetic and mechanical properties. In this work, it is shown that the presence of MS particles around larger MH particles, firstly, causes an augmentation of magnetic moments, which the MH particles acquire during initiation, and secondly, enhances the magnetic susceptibility and remanent magnetisation of MAEs-MC. These magnetic parameters are evaluated on the basis of the macroscopic magnetostatics from the experimental data of spatial scanning of the field over the space around MAEs-MC made in the shape of a spheroid. A set of samples with a fixed MH and varying MS volume contents that are initiated in two different fields, is used. The developed mesoscopic model of magnetic interactions between the MH and MS phases is able to explain the experimentally observed dependencies of the magnetic parameters on the concentration of the MS phase. The problem is solved numerically under the assumption that the elastic matrix of MAEs-MC is rigid, i.e. the mutual displacements of the particles are negligible. The model helps to elucidate the interaction of the magnetic phases and to establish that the MS phase plays thereby a dual role. On the one hand, the MS phase screens out the field acting inside MH particles, and on the other hand, it forms mesoscopic magnetic bridges between adjoining MH particles, which in turn enhance their field. The combined interplay of these contributions defines the resulting material properties of MAEs-MC on the macroscopic scale.

Original Content from this work may be used under the terms of the Creative Commons Attribution 4.0 licence. Any further distribution of this work must maintain attribution to the author(s) and the title of the work, journal citation and DOI.

Keywords: magnetoactive elastomer, mixed magnetic content, remanent magnetisation, magnetic susceptibility, mesoscopic model cell, magnetic interaction

(Some figures may appear in colour only in the online journal)

1. Introduction

Magnetoactive elastomeric composites of mixed magnetic content are rather different from both their 'predecessors': magnetoactive elastomers (MAEs) filled exclusively with micropowders of either a magnetically soft (MS) or a magnetically hard (MH), i.e. highly coercive, ferromagnetic material. These two types of composites are quite well known nowadays. The literature on physics and mechanics of MAEs of the MS type is really vast, and one is able to name just a few benchmark works [1–11]. The interest to MAEs of the MH type has arisen much later, but by now the reference list is rather lengthy as well. Here we refer to only some notable papers [12–21]. Note that under the latter term we imply real elastomers (soft materials) and not traditional magnetic rubbers, the material science of which counts a long period of development.

The idea of the magnetoactive elastomers of mixed magnetic content, see figure 1 – in what follows we denote them as MAEs-MC—is rather new [22–26]. Their novel qualities stem from the fact that in such composites the magnetic interaction occurs not only from the coupling of each fraction of the particles with external field and within the same fraction. An important contribution, which their magnetomechnanics benefits from, is the magnetic interaction between the MH and MS phases. As a magnetised MH grain is a point-dipole-like source, its field decays fast with the distance from its centre. Therefore, for an efficient MH–MS coupling inside a composite, the magnetic moment of an MH grain should be as large as possible under a given restriction on the particle size (tens of microns). Provided the extent of coupling is sufficient, the magnetomechanical properties of an MAE-MC sample might be tuned in two ways. For one thing, the *passive tuning* is attained by the level of initial magnetisation endowed to the MH particles. On the other hand, the *active tuning* under the action of externally applied field is available as for any usual MAE filled just with an MS powder. Evidently, this double control over mechanics, including rheology, is a unique quality acquired by such composites due to their mixed magnetic content [23, 26, 27].

In this connection, an important remark should be made. At present, two types of the micron-size MH particles are in experimental use for MAEs: either barium hexaferrite [14, 16, 17, 21] or NdFeB [15, 22–26]. Given that the saturation magnetisations in the bulk state are about 350 kA m^{-1} and 1300 kA m^{-1} for $BaFe_{17}O_{19}$ and $Nd_2Fe_{14}B$, respectively, it is clear that MAEs-MC with an MH filler made of NdFeB are much prospective for applications. That is why below we focus on the composites with the latter type of the MH phase.

Since the MH microparticles are introduced into a composition in a non-magnetised state, and the polymerisation of the sample takes place in the absence of external field, there are no small-scale (mesoscopic) magnetic fields inside a synthesised elastomeric composite. It is at the final stage of its preparation, that an MAE-MC sample is placed inside a powerful electromagnet and treated for a short time with a large magnetic field. We term this external field as 'initiating' and denote it by $\boldsymbol{H}_{\rm ext}^{\rm ini}$. Once it is switched off, the MAE-MC sample acquires a remanent magnetisation M_R along the direction $\mathbf{n} = \boldsymbol{H}_{\rm ext}^{\rm ini}/H_{\rm ext}^{\rm ini}$.

In this work we predict and demonstrate that in real magnetised MAEs-MC, a strong interaction of the MH and MS phases takes place, and the properties of such a composite are substantially non-additive. For that, in section 2, using some available experimental evidence, we discuss qualitatively the magnetomechanics of such a material system with emphasis on the twofold role of the MS phase, especially under conditions where MH particles do not attain full magnetic saturation. The role of magnetomechanical hysteresis on the macroscopic properties of MAEs-MC is beyond the scope of the present paper. In a general case, when the composite matrix is soft, the magnetomechanical hysteresis manifests itself and requires modelling of the effect of the particle collapsing toward each other as observed in [28–30]. We address the case of sufficiently stiff composite matrix, which virtually excludes spatial freedom of the particles of any type. In section 3 – in order to elucidate the origin of the magnetic properties of MAEs-MC—we propose an appropriate mesoscopic model to analyse the magnetic response of these composites. With the aid of it, first, the case of a composite filled only with MH particles is analysed. We develop a procedure to describe the 'initiation' scenario—when a freshly prepared sample is subjected to a large field—and then consider the resulting state of the remanent magnetisation. Both these steps imply substantial numeric calculations. In the second part of section 3, the model description is extended to the case of mixed (MH + MS) magnetic content. The set of magnetostatic equations pertinent to the model is presented, the way of solving them is outlined, and reference examples which demonstrate, how the presence of the MS phase affects both the initiation and the remanent magnetisation of MAEs-MC, are given.

Preparation of the MAEs-MC for experimental tests—from mixing of components to accomplishment of initiation, i.e. imparting a remanent magnetisation to the synthesised samples—is detailed in section 4. The geometric parameters of the moulded samples in the shape of a spheroid are given together with the proportions of their MH and MS volume contents. As well, the procedure of measurement of the magnetic field in the space around the sample is described.

In section 5, on the basis of macroscopic magnetostatics the relations are obtained that enable one to extract from the primary measurement data the magnetic material parameters, i.e. the net susceptibility and remanent magnetisation, of a particular MAE-MC initiated by an external field of given strength. As all the experimental samples contain equal

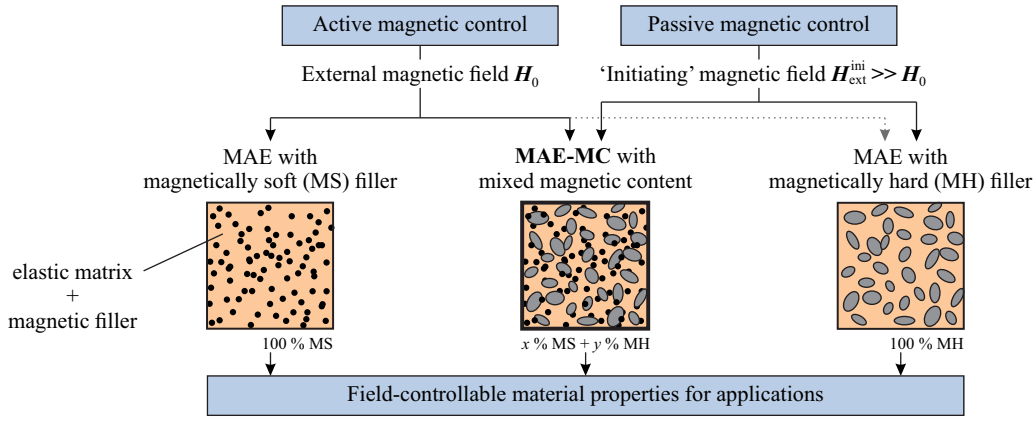

Figure 1. Types of MAE composites according to magnetic filling.

amount of the MH phase, the encountered difference in magnetic properties is ascribed to variation of the volume content of the MS phase. The mesoscopic model developed, as a general scheme, in sections 2 and 3, is used in section 6 to explain the experimentally obtained dependencies on the MS concentration and is proven to be quite adequate for handling the problem.

2. Qualitative aspects of the magnetic state of an MAE-MC

The reference sizes of microparticles, which constitute the mixed ferromagnetic filler of MAEs-MC, differ, as a rule, by approximately an order of magnitude: 30–50 μm for MH particles and 3–5 μm for MS ones, so that the particle volumes differ about thousand times. Due to that, one may assume that in an MAE-MC that contains comparable amounts of the magnetic phases, the provided components had been well mixed before curing, and each MH particle is surrounded by a matrix region that contains a large number of MS particles.

As soon as—in result of the 'initiating' magnetisation—an MH particle acquires a magnetic moment, it polarises the surrounding MS particles and, thus, redistributes the local magnetic flux. Consider a simple idea of an elementary structure unit of an MAE-MC as a solitary MH particle enveloped by a spherical layer of a polymer matrix, inside which the MS particles are dispersed.

The magnetic shielding, i.e. partial closure of the magnetic flux of the MH particle produced by its MS shell, should be the main effect here. Given that, the magnetic field outside the considered unit is the weaker the higher volume concentration of the MS particles ϕ_{MS}. Extending this inference to a macroscopic MAE-MC sample, one may conclude that the observed magnetic moment of the sample with a fixed amount of the MH phase will gradually decrease as the MS phase is added.

However, the measurement results that are presented in full in section 5 establish exactly the opposite tendency: the observed magnetic moment of the sample grows with the increase of ϕ_{MS}. This evidences that in MAEs-MC, the interaction of the MH and MS phases cannot be ascribed just to the shielding effect and has a more complex character.

The magnetic properties of MAEs-MC depend essentially on the type of MH component. In our experiments we use spherical NdFeB particles from Magnequench (magnet powder MQP-S-11-9-20 001-070) [31]. From a conventional point of view, each such MH particle is a solid clot of single-domain nanograins with randomly distributed directions of their uniaxial anisotropy axes. The magnetisation of the afore-mentioned NdFeB particles comes to true saturation only in a strong magnetising field H_{ext}^{ini} of $\sim$ 3.2–5.6 MA m^{-1}, which is not available under usual laboratory conditions. Standard electromagnet facilities, which we use to prepare MAE-MC samples, allow one to obtain $H_{ext}^{ini} \lesssim 2$ MA m^{-1} at a maximum. Moreover, if to make inside an electromagnet a room to place a sample of 20–30 mm in size, the available uniform field does not exceed 1.2 MA m^{-1}. Under such treatment, the MH particles do not attain full saturation but magnetise along some minor (partial) hysteresis loops. Because of that, under the peak field value H_{ext}^{ini}, the level of magnetisation that MH particles attain, is significantly lower than the possible maximum (saturation) that in our case is $M_{MH}^{(sat)} = 1280$ kA m^{-1} [32].

The direct proof of that follows from the dependence of the macroscopic remanent magnetisation M_R on the field strength H_{ext}^{ini} shown in figure 2 for an MAE containing only MH microparticles of the above-mentioned type. To compare the measurement results for samples with two different concentrations, the obtained data are normalised to 100 % volume content of NdFeB. As it is seen, the maximum accessible field of 2 MA m^{-1} produces a remanent magnetisation of particles of about 500 kA m^{-1}, and about 400 kA m^{-1} in a field of 1.2 MA m^{-1}, see figure 2.

Note that with allowance for the specifics of the MH particles, i.e. optimally quenched $Nd_{14}Fe_{80}B_6$ (Magnequench), the magnetisation values given in figure 2 should not be compared with the prediction of the Stoner–Wohlfarth model for an assembly of spherical particles with randomly distributed anisotropy axes. As is known, the latter model gives a remanence value of $M_R = \frac{1}{2}M_{MH}^{(sat)}$ [33], i.e. 640 kA m^{-1} in our case. A more correct comparison should take into account the experimental fact that for the afore-mentioned NdFeB particles, the remanence is about 6 % higher than the classical

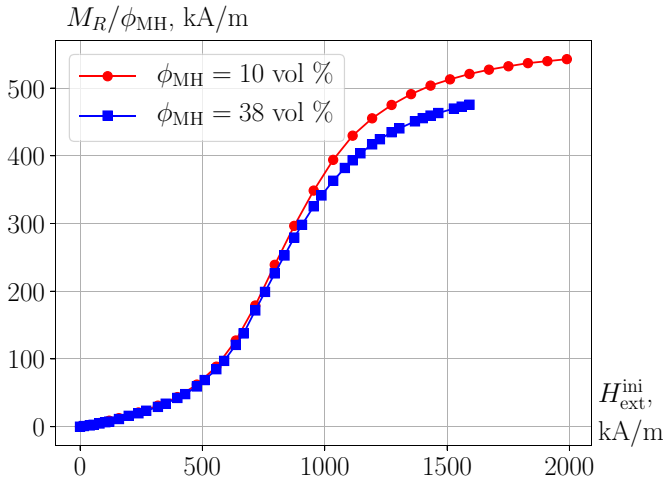

Figure 2. Dependence of the remanent magnetisation of MAEs containing spherical MH particles of NdFeB (Magnequench) on the strength of the initiating magnetic field for volume concentrations ϕ_{MH} of 10 % and 38 %; data are normalised to 100 % volume content of the MH phase.

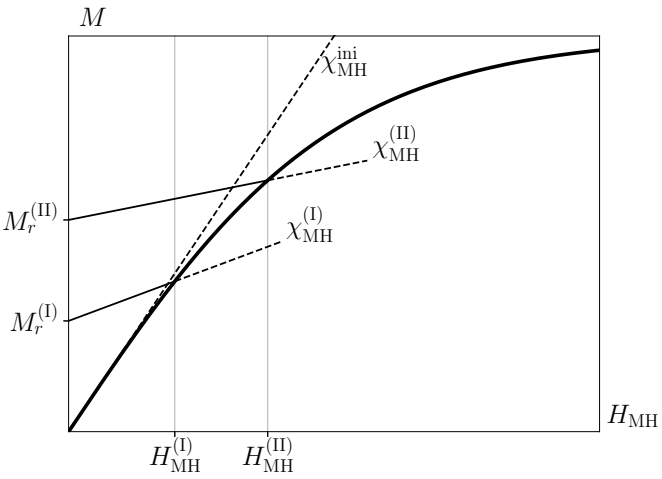

Figure 3. Schematic diagram of the MH particle magnetisation along the initial magnetisation curve (thick line) and partial hysteresis loops (thin lines). The magnetic susceptibility of the initial magnetisation always exceeds those of the subsequent ones: $\chi^{\mathrm{ini}}_{\mathrm{MH}} > \chi^{(\mathrm{I})}_{\mathrm{MH}} > \chi^{(\mathrm{II})}_{\mathrm{MH}}$, see the slopes of the dashed lines.

estimation that in our case yields $M_{\mathrm{lim}} = 676\,\mathrm{kA\ m^{-1}}$ [32]. Thus, even in a field of 2 MA m^{-1}, the studied MAE samples acquire the remanent magnetisation that does not exceed 78 % of the attainable maximum that is a clear indication that the magnetisation cycle is a partial one. The consequence of this incomplete magnetisation is the strong field dependence of the remanence M_r of a single MH particle. The effect is illustrated schematically in figure 3, where the horizontal axis corresponds to the field H_{MH} acting on the MH particle inside an MAE. The increase of this field from $H^{(\mathrm{I})}_{\mathrm{MH}}$ to $H^{(\mathrm{II})}_{\mathrm{MH}}$ leads to the growth of the remanent magnetisation from $M_r^{(\mathrm{I})}$ to $M_r^{(\mathrm{II})}$. The existence of such dependence is qualitatively proven by the macroscopic data presented in figure 2, where at moderate field strengths the curves $M_R(H^{\mathrm{ini}}_{\mathrm{ext}})$ are quite steep. In particular, when the field increases from 600 to 1200 kA m^{-1}, the value of M_R grows by about 4.5 times.

Another important experimental evidence that follows from the measurements of $M_R(H^{\mathrm{ini}}_{\mathrm{ext}})$, is its weak dependence on the concentration ϕ_{MH} of the MH phase. Despite the almost fourfold concentration difference between the samples, the obtained curves $M_R(H^{\mathrm{ini}}_{\mathrm{ext}})$ differ not greater than by 15 %. Moreover, our experience of working with MAEs, suggests that this difference should be rather associated with inaccuracy of determining the initial material parameters, e.g. density of the powder, and with measurement errors.

One should expect that the strong dependence $M_R(H^{\mathrm{ini}}_{\mathrm{ext}})$ of the micron-size MH particles revealed experimentally on elastomers without an MS phase, should play an important role in magnetisation of composites with a mixed content. Consider a long rod made of a just prepared MAE-MC, but not yet magnetised. In this case, the shape effect causing a demagnetising field is absent, and the resulting magnetic response is essentially the response of the material itself. Let the magnetisation process to be at the beginning, so that the initiating field has a moderate magnitude, say, of 240 kA m^{-1}. Using the data of figure 2 for estimations, one concludes that such a field induces a weak magnetisation of the MH particles: about 25 kA m^{-1}. However, for MS particles of a carbonyl iron powder (CIP), the same field is rather strong, and it brings their magnetisation almost up to a saturation value $M_{\mathrm{CIP}} \sim 1600\,\mathrm{kA\ m^{-1}}$. As a result, the additional internal field created by MS particles on the MH particle is of the order of $\Delta H_{\mathrm{MH}} \sim M^{(\mathrm{sat})}_{\mathrm{MS}} = \phi_{\mathrm{MS}} M_{\mathrm{CIP}}$. This points out that in an MAE-MC sample with a CIP content $\phi_{\mathrm{MS}} \sim 10\,\%$, the internal field exceeds the external one by $\Delta H_{\mathrm{MH}} \sim 160\,\mathrm{kA\ m^{-1}}$.

Due to the fast saturation of the MS phase, the value of ΔH_{MH} remains almost unchanged with further growth of the external field $H^{\mathrm{ini}}_{\mathrm{ext}}$. Being proportional to the MS concentration, this contribution might be treated as some bias field. Within the range 240–400 kA m^{-1}, the change of the field $H^{\mathrm{ini}}_{\mathrm{ext}}$ by an increment of $\Delta H_{\mathrm{MH}} \sim 80$–$160\,\mathrm{kA\ m^{-1}}$ causes only a small change in M_R. However, as figure 2 shows, in the range of 600–1200 kA m^{-1} the characteristic curve is rather steep, so that the same bias field $\Delta H_{\mathrm{MH}} \propto \phi_{\mathrm{MS}}$ can significantly increase the attained value of the remanent magnetisation M_R.

From the afore-mentioned considerations an important conclusion can be drawn that applies to any MAE-MC no matter what is the actual proportion between the MH and MS phases:

> *When an MAE-MC is subjected to an external magnetic field that does not bring the embedded MH particles to complete saturation, one should take into account that the internal field acting on these particles, exceeds the external one by an amount proportional to the concentration of the MS phase.*

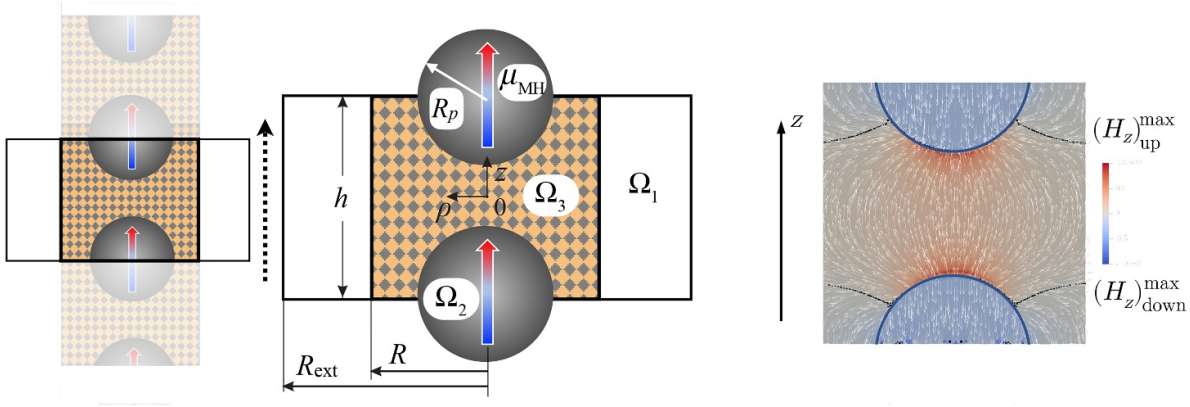

Figure 4. Scheme of the mesostructure model cell of an MAE-MC after processing by an 'initiating' magnetic field: grey spheres are MH particles; dotted region is the matrix containing MS particles; black frame indicates a recurring structure element used for numeric calculation. The rightmost panel shows the distribution of z-component of the internal magnetic field in the basic state of the cell (initiating field is switched off); this field component is zero along divergent lines.

3. Mesoscopic modelling of an MAE-MC

3.1. Model cell

The applied uniform magnetic field generates inside MH particles of an MAE-MC sample a field $\boldsymbol{H}^{\rm ini}_{\rm MH}$, which imparts to them a remanent magnetisation. These fields differ from each other not only due to the overall shape effect (demagnetisation), but also due to the presence of local fields created by MS particles. Moreover, demagnetising fields of the sample during the initial and subsequent magnetisations are different on account of the fact that the MH particles have different magnetic susceptibilities before and after the initial magnetisation, see slopes of the lines $M_r(H_{\rm MH})$ in the vicinity of the ordinate axis in figure 3. Evidently, in order to evaluate correctly the remanent magnetisation of an MAE-MC, all indicated effects of the MH and MS phase interactions should taken in consideration.

In a sample without MS phase and a moderate concentration of the MH phase, the macroscopic remanent magnetisation can be estimated as $M_R \approx \phi_{\rm MH} M_r$, where $M_r(H^{\rm ini}_{\rm MH})$ is the remanent magnetisation of an MH particle caused by the field $H^{\rm ini}_{\rm MH}$ acting inside it. A different situation takes place in an MAE-MC sample containing the fillers of both types. First, the external (initiating) field affects MS particles, and they contribute to the field $H^{\rm ini}_{\rm MH}$. Therefore, MH particles are magnetised differently than in the case of $\phi_{\rm MS} = 0$. Once the applied field is turned off, the MH particles become autonomous field sources and polarise their MS environment. Due to the fact that the field generated by each MH particle is non-uniform, this polarisation influences the macroscopic remanent magnetisation M_R in two ways, as shown schematically in figure 4.

There a fragment of an MAE-MC composite is presented as a cylindrical column of radius R, which contains a sequence of MH particles of radius R_p possessing magnetic moments $\boldsymbol{\mu}_{\rm MH}$ directed along the direction of the magnetising field. The MH particles are located at the axis of the column at equal distances, and the recurring element is selected so that two adjoining particles enter it. The period of this mesostructure is h. It is assumed that the column has infinite length, making possible to neglect the demagnetising factor of the sample. The residual part of the column space is filled up with the elastic matrix containing MS particles. The cylindrical region of radius $R_{\rm ext}$ around the column is considered empty and needed for correct execution of the numerical calculations.

The schemes in figure 4 point out the two essential features of the model. On the one hand, the magnetic flux of each MH particle locks to some extent through the surrounding MS phase, and this causes the shielding effect. The regions lying near the equatorial belt of each MH particle make an important contribution, since there the field generated by the particle is antiparallel to its magnetic moment $\boldsymbol{\mu}_{\rm MH}$, that is the direction of the magnetisation. Clearly, the shielding pattern is equivalent to a kind of domain structure and, thus, reduces the remanent magnetisation of the MAE-MC. On the other hand, since the magnetic moments of the neighbouring MH particles are in the head-tail configuration, the matrix regions between them filled with MS particles act as magnetic circuits connecting these permanent magnets. The existence of such magnetic circuits increases the remanent magnetisation of the sample in comparison with the value that it would have in a material with the same concentration $\phi_{\rm MH}$, but at $\phi_{\rm MS} = 0$. Therefore, one sees that the macroscopic magnetisation of an MAE-MC, where the MS phase is present, acquires the corrections, which counteract each other.

Since the model cell is assumed to be a part of an infinite system, there is no difference between the external field $H^{\rm ini}_{\rm ext}$ and the field acting inside the material. However, when describing the initiation stage of a real system, one should discriminate between $H^{\rm ini}_{\rm ext}$ and $H^{\rm ini}_0$ that is the field existing inside the finite sample. These fields are related to each other as

$$H^{\rm ini}_0 = H^{\rm ini}_{\rm ext} - \mathcal{N}_z M^{\rm ini}(H^{\rm ini}_0, \phi_{\rm MS}), \qquad (1)$$

where $M^{\rm ini}$ is the net magnetisation of the composite at the initiating magnetisation, $\mathcal{N}_z$ is the demagnetisation factor of the sample. We will recall this condition in section 6 when discussing evaluation of the magnetic properties of MAEs-MC on the basis of measurements made on spheroidal samples.

3.2. Remanent magnetisation of a composite with only MH phase

To find the remanent magnetisation of an MAE containing MH phase, one needs to accomplish two steps:

(a) computation of the field $\boldsymbol{H}_{\rm MH}^{\rm ini}$ generated in an initially non-magnetised MH particle by an external field $\boldsymbol{H}_0^{\rm ini}$ acting on the model cell;
(b) calculation of the field distribution in the model cell after the initiating field $\boldsymbol{H}_0^{\rm ini}$ is turned off; from these data the remanent magnetisations of each MH particle and the model cell are evaluated.

To carry out the numerical calculation, the model cell is divided into three subregions: Ω_1 – empty space; Ω_2 – the MH particle that has zero magnetisation and susceptibility $\chi_{\rm MH}^{\rm ini}$ before the field $\boldsymbol{H}_0^{\rm ini}$ is applied, and magnetisation $\mathbf{M}_r(\boldsymbol{H}_0^{\rm ini})$ and susceptibility $\chi_{\rm MH}$ after this field has been switched off; Ω_3 – the matrix containing MS particles (figure 4). The geometric parameters are selected in such a way that the radius of the MH particle is taken as the unit length. This renders the dimensionless distances in the form: $R_p = 1, R = 1.88, h = 2$ R, $R_{\rm ext} \geq 5$ R. With these values, the volume concentration of the MH phase in the cell is $\phi_{\rm MH} = 10\,\%$ that corresponds to MAEs-MC used in our measurements reported below.

In the present section, we consider the case when the MS phase is absent: $\phi_{\rm MS} = 0$ that substantially simplifies the calculation process. The solution of the corresponding magnetostatic problem is obtained by the finite element method and takes into account the demagnetisation of a spherical MH particle, which is proportional to $\chi_{\rm MH}^{\rm ini}$, i.e. the slope of the initial magnetisation curve in figure 3. It is assumed that $\chi_{\rm MH}^{\rm ini}$ does not depend on the magnitude of the initiating field. Moreover, in what follows it is set that this susceptibility does not depend on the presence of the MS phase. Under these assumptions and with periodic boundary conditions, the function $H_{\rm MH}^{\rm ini}(H_0^{\rm ini})$ is obtained, which defines the field strength acting inside the MH particle in the model cell, when the latter is exposed to a uniform field $H_0^{\rm ini}$. Due to the low MH concentration and small initial susceptibility $\chi_{\rm MH}^{\rm ini}$, this solution does not differ much from the analytical solution of the corresponding single-particle problem:

$$H_{\rm MH}^{\rm ini} = H_0^{\rm ini} \Big/ \left(1 + \tfrac{1}{3}\chi_{\rm MH}^{\rm ini}\right). \tag{2}$$

Figure 5 presents the comparison of the numeric and analytical solutions of $H_{\rm MH}^{\rm ini}(H_0^{\rm ini})$ for a susceptibility value of $\chi_{\rm MH}^{\rm ini} = 0.63$, which is specified by approximating experimental data of the initial magnetisation measured for the MAE samples containing only MH particles.

Further calculations can be greatly simplified by employing an approximate analytical representation of the remanent magnetisation $M_r\left(H_{\rm MH}^{\rm ini}\right)$ of an MH particle. A plausible form for that we build up on the basis of the Langevin function $\mathcal{L}(z) = \coth z - 1/z$ because it saturates by definition and has a simple mathematical form. Clearly, this approximation is by no means the only one possible. The Langevin function with a modified argument

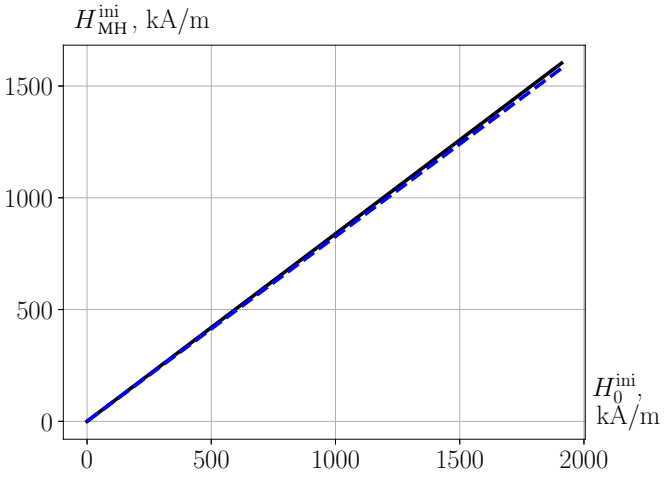

Figure 5. Dependence of the field inside the MH particle on the initiating field for an MH susceptibility of $\chi_{\rm MH}^{\rm ini} = 0.63$: solid line—numerical computation using the model cell; dashed line—solution (2) of the one-particle problem.

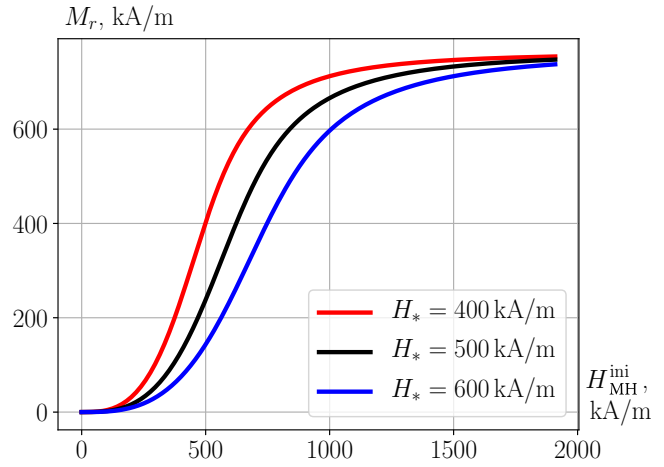

Figure 6. Model approximation curves $M_r(H_{\rm MH}^{\rm ini})$ defined by (3) for $M'_{\rm lim} = 761$ kA m^{-1} and three different values of H_*.

$$M_r(H_{\rm MH}^{\rm ini}, H_*) = M'_{\rm lim}\mathcal{L}\left([H_{\rm MH}^{\rm ini}/H_*]^3\right) \tag{3}$$

provides a good description of the curves shown in figure 2 almost everywhere, except for the region of weak fields that is of no particular interest here. In (3), $M'_{\rm lim}$ is the limiting value of the magnetisation of the MH phase, and H_* is a scaling coefficient to be determined. Expectedly, the dependencies of the remanent magnetisation on the fields $H_0^{\rm ini}$ and $H_{\rm MH}^{\rm ini}$ do not differ from each other in the qualitative aspect.

The characteristic behaviour of function (3) and its dependence on the parameter H_* are illustrated in figure 6. The resemblance between these approximation curves and the experimental ones in figure 2 is evident. Further on, it is assumed that expression (3) retains its form regardless of what sources generate the internal magnetic field.

At the step (b), when the initiating field $H_0^{\rm ini}$ is turned off, and the magnetised MH particles remain the only field sources, the problem of the field distribution inside the model cell is

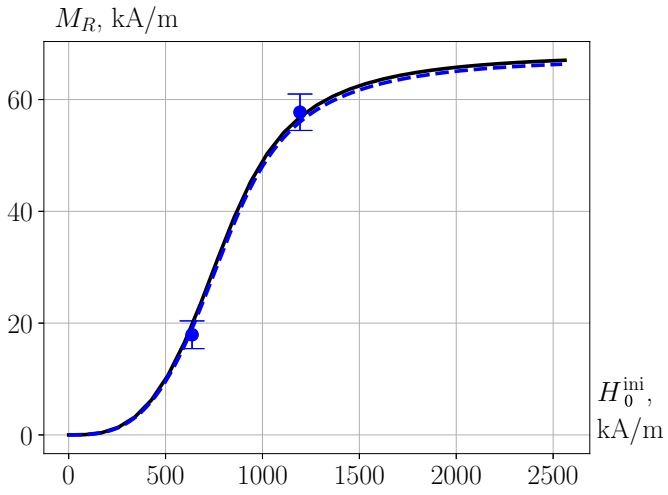

Figure 7. Remanent magnetisation of an MAE with $\phi_{\text{MH}} = 10\,\%$ depending on the external field H_0^{ini} for $M'_{\text{lim}} = 761\,\text{kA m}^{-1}$, $H_* = 547.5\,\text{kA m}^{-1}$, $\chi_{\text{MH}}^{\text{ini}} = 0.63$ and $\chi_{\text{MH}} = 0.38$: solid line—numerical result for the model cell; dashed line—solution (4) of the single-particle problem; markers—experimental results for the spheroidal sample No. 1 magnetised in fields of 637 kA m^{-1} and 1194 kA m^{-1}.

solved with the same numerical technique. The remanent magnetisation M_r of each MH particle is found taking into account that now the demagnetising field is defined by the magnetic susceptibility χ_{MH} that is lower than the initial one $\chi_{\text{MH}}^{\text{ini}}$, see figure 3. Then, the remanent magnetisation of the whole cell M_R is calculated. This value can be also approximated by the solution of the corresponding single-particle problem:

$$M_R(H_0^{\text{ini}}) = \frac{\phi_{\text{MH}} M'_{\text{lim}}}{1 + \frac{1}{3}\chi_{\text{MH}}}\,\mathcal{L}\left(\left[\frac{H_0^{\text{ini}}}{(1+\frac{1}{3}\chi_{\text{MH}}^{\text{ini}})H_*}\right]^3\right). \quad (4)$$

The saturated remanent magnetisation M_{lim} of the spherical particle is related to the limiting magnetisation of its material M'_{lim} as

$$M_{\text{lim}}\left(1 + \tfrac{1}{3}\chi_{\text{MH}}\right) = M'_{\text{lim}}; \quad (5)$$

for $\chi_{\text{MH}} = 0.38$ and $M_{\text{lim}} = 676\,\text{kA m}^{-1}$, one gets $M'_{\text{lim}} = 761\,\text{kA m}^{-1}$, which will be used in further calculations.

The value of scaling parameter $H_* = 547.5\,\text{kA m}^{-1}$ in (3) is chosen on the best fit basis upon comparing the model dependence $M_R(H_0^{\text{ini}})$ with experimental measurements for the MAE samples with $\phi_{\text{MH}} = 10\,\%$ and $\phi_{\text{MS}} = 0\,\%$. As figure 7 shows, the match between the numerical and analytical (single-particle problem) solutions is rather good. Note that H_* qualitatively corresponds to a reference field strength, beyond which the magnetisation curve $M_R(H_0^{\text{ini}})$ becomes most steep.

3.3. Remanent magnetisation of a composite with both MH and MS phases

Inside the model cell shown in figure 4, the MS phase occupies the region Ω_3. Since the particles of this component are at least an order of magnitude smaller the MH ones, the region Ω_3 is modelled as an MS continuum that is magnetised reversibly according to the non-linear Fröhlich–Kennelly law with the susceptibility [34]:

$$\chi_{\text{MS}}(H) = \frac{\chi_{\text{MS}}^0 M_{\text{MS}}^{(\text{sat})}}{M_{\text{MS}}^{(\text{sat})} + \chi_{\text{MS}}^0 H}. \quad (6)$$

Here, χ_{MS}^0 is the initial susceptibility of the MS phase, and $M_{\text{MS}}^{(\text{sat})}$ is its saturation magnetisation, which is expressed by $M_{\text{MS}}^{(\text{sat})} = \overline{\phi}_{\text{MS}} M_{\text{CIP}}$. The volume concentration of MS particles $\overline{\phi}_{\text{MS}}$ in the region Ω_3 is identified from the macroscopic measurements and related to the MS concentration in the entire cell through the ratio of volumes:

$$\phi_{\text{MS}} = \frac{V_{\Omega_3}}{V_{\Omega_2} + V_{\Omega_3}}\,\overline{\phi}_{\text{MS}}.$$

The concentration dependence of the susceptibility χ_{MS} is approximated by the Lichtenecker formula [35], which is quite reliable for composites with an MS volume content up to 30 %:

$$\chi_{\text{MS}}^0 = (\mu_{\text{e}})^{\overline{\phi}_{\text{MS}}} - 1, \quad (7)$$

where μ_{e} is the effective initial magnetic permeability of the MS phase.

The magnetostatic problem in the absence of charges and currents is described by two Maxwell equations and two boundary conditions following from them:

$$\nabla \times \boldsymbol{H} = 0, \quad \nabla \cdot \boldsymbol{B} = 0, \quad [\boldsymbol{H}_\tau] = 0, \quad [B_n] = 0. \quad (8)$$

Here, $\boldsymbol{B}$ is the magnetic flux density, subscripts n and τ mark the normal and tangential components of a vector at a surface of discontinuity, whereas square brackets denote the difference between the corresponding values on two sides of this boundary.

The first equation of (8) shows that $\boldsymbol{H}$ is a potential field, which can be expressed as a superposition of an external uniform field $\boldsymbol{H}_0$ and gradient of a scalar potential ψ:

$$\boldsymbol{H} = \boldsymbol{H}_0 - \nabla\psi. \quad (9)$$

Note that hereinafter the field $\boldsymbol{H}_0$ may play one of two distinctive roles. It is either a strong initiating field $\boldsymbol{H}_0^{\text{ini}}$ imposed on an MAE-MC during primary magnetisation and imparting to the MAE-MC composite a macroscopic remanent magnetisation M_R. Or it might be an external field $\boldsymbol{H}_0$ of relatively weak strength ($H_0 \ll H_0^{\text{ini}}$) applied to a magnetised (initiated) MAE-MC in order to tune actively its material properties, see section 5 for more on this subject.

We consider a rotationally symmetric model cell, so that the potential ψ depends only on the radial distance ρ and axial coordinate z, see figure 4. Then the function $\psi(\rho, z)$ should, first, vanish at the cylindrical boundary of the cell: $\psi\big|_{\rho=R_{\text{ext}}} = 0$; and, second, be periodic along the Oz axis: $\psi(\rho, z) = \psi(\rho, z + h)$, where h is the cell period.

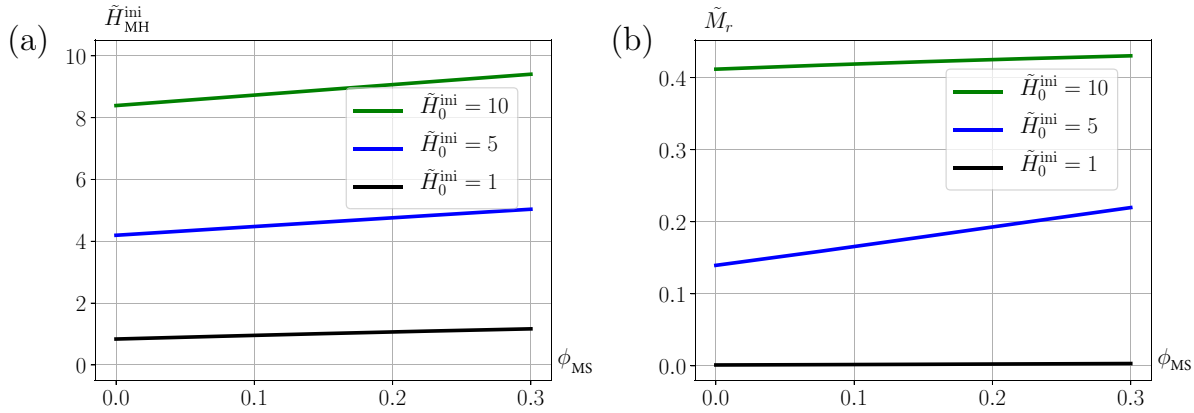

Figure 8. Theoretical dependencies: (a) of the magnetic field acting inside an MH particle and (b) its remanent magnetisation acquired after treatment by the initiating field $\tilde{H}_0^{\rm ini}$ (shown in dimensionless form) as functions of the MS phase content.

The solution of (8) is equivalent to the problem of seeking an extremum (here, a maximum) of the energy functional [36]

$$\int_V \boldsymbol{B}\cdot\delta\boldsymbol{H}\,dV=0 \tag{10}$$

for the cell of volume V.

The vector of the magnetic flux density (induction) is defined in each subregion of the model cell as

$$\boldsymbol{B}=\begin{cases}\mu_0\,(\boldsymbol{H}_0-\nabla\psi) & \text{for } \Omega_1,\\ \mu_0\,(1+\chi_{\rm MH})\,(\boldsymbol{H}_0-\nabla\psi)+\mu_0\boldsymbol{M}_r & \text{for } \Omega_2,\\ \mu_0\,(1+\chi_{\rm MS}(H))\,(\boldsymbol{H}_0-\nabla\psi) & \text{for } \Omega_3,\end{cases} \tag{11}$$

where μ_0 is the magnetic permeability of vacuum.

Taking into account the relations between variations of the thermodynamic quantities

$$\delta\boldsymbol{H}=-\nabla\delta\psi \quad \text{and} \quad \int_V \boldsymbol{H}_0\cdot\nabla\delta\psi\,dV=0,$$

one can see that (10) can be transformed to the following variational equation

$$\begin{aligned}\int_V \nabla\psi\cdot\nabla\delta\psi\,dV=&\int_{V_{\Omega_2}}(\chi_{\rm MH}(\boldsymbol{H}_0-\nabla\psi)+\boldsymbol{M}_r)\cdot\nabla\delta\psi\,dV\\&+\int_{V_{\Omega_3}}\chi_{\rm MS}(H)\,(\boldsymbol{H}_0-\nabla\psi)\cdot\nabla\delta\psi\,dV,\end{aligned} \tag{12}$$

where V_{Ω_2} and V_{Ω_3} are the volumes of the MH particle and region occupied by the MS phase, respectively. This variational problem is solved numerically for function $\psi(\rho,z)$ using finite element algorithms implemented in *Python* programming language with *FEniCS* computing platform [37].

At the step (a) of the initiating magnetisation, the solution of (12) is found by assuming that $H_0^{\rm ini}\gg M_{\rm CIP}$ and $M_r=0$. The result provides the distribution of the potential $\psi(\rho,z)$ in the entire computational region of the cell. Then, the vector field $\boldsymbol{H}=\boldsymbol{H}_0-\nabla\psi$ is averaged over the volume V_{Ω_2} occupied by the MH particle according to

$$\boldsymbol{H}_{\rm MH}^{\rm ini}=\frac{1}{V_{\Omega_2}}\int_{V_{\Omega_2}}(\boldsymbol{H}_0-\nabla\psi)\,dV. \tag{13}$$

Transition to dimensionless units for the magnetic quantities is done by normalising them to the saturation magnetisation $M_{\rm CIP}=1600\,{\rm kA\,m^{-1}}$ of the MS phase. Upon marking the dimensionless quantities by tildes, one has for any magnetic field strength $\tilde{\boldsymbol{H}}=4\pi\boldsymbol{H}/M_{\rm CIP}$ and for the magnitude of any magnetisation $\tilde{\boldsymbol{M}}=\boldsymbol{M}/M_{\rm CIP}$.

Let us proceed to the results of numerical computation of the dependence $\tilde{H}_{\rm MH}^{\rm ini}(\tilde{H}_0^{\rm ini})$ for different values of the MS volume concentration $\phi_{\rm MS}$. For the case $\phi_{\rm MS}=0$, this dependence is described in section 3.2 and shown in figure 5. The following parameters are used in calculations:

$$\begin{aligned}&\phi_{\rm MH}=0.1,\ \chi_{\rm MH}^{\rm ini}=0.63,\ \chi_{\rm MH}=0.38,\ M'_{\rm lim}=761\,{\rm kA\,m^{-1}},\\&H_*=547.5\,{\rm kA\,m^{-1}}\quad\text{and}\quad\mu_{\rm e}=80.\end{aligned} \tag{14}$$

As can be seen in figure 8(a), the presence of the MS phase enhances notably the field $H_{\rm MH}^{\rm ini}$ acting inside an MH particle, in comparison with the case where the MS phase is absent. The emerging field $H_{\rm MH}^{\rm ini}$, due to the demagnetising effect, is always smaller than the initiating field $H_0^{\rm ini}$. In particular, the field with magnitude of $H_0^{\rm ini}=637\,{\rm kA\,m^{-1}}$ (the corresponding dimensionless value is 5) generates inside an MH particle the fields of magnitudes $533\,{\rm kA\,m^{-1}}$ and $637\,{\rm kA\,m^{-1}}$ (4.2 and 5 in dimensionless units) for concentrations $\phi_{\rm MS}=0$ and 0.3, respectively.

At the step (b), when the initiating field $\boldsymbol{H}_0^{\rm ini}$ is turned off, the remanent magnetisations of the MH particle and model cell are calculated by solving (12). The value $\phi_{\rm MS}$ is fixed, and with it the corresponding function $\chi_{\rm MS}(H)$ is determined; also the initial susceptibility $\chi_{\rm MH}^{\rm ini}$ is replaced by its value $\chi_{\rm MH}<\chi_{\rm MH}^{\rm ini}$. Figure 8(b) shows the obtained MH particle remanence M_r dependent on the volume concentration of the MS phase. The slopes of these lines are easy to interpret qualitatively. For $\tilde{H}_0^{\rm ini}=1$, the MH particles are weakly magnetised, and therefore, the line $\tilde{M}_r(\phi_{\rm MS})$ is almost horizontal. In a field of $\tilde{H}_0^{\rm ini}=5$, the line has a maximum slope. The obvious reason for it is that under moderate fields, the bias field $\Delta H_{\rm MH}$ induced by $H_0^{\rm ini}$ in the MS phase enhances most effectively the remanent magnetisation of MH particles. Higher magnetic fields, e.g. $\tilde{H}_0^{\rm ini}=10$, slow down the growth of the magnetisation $\tilde{M}_r$ since

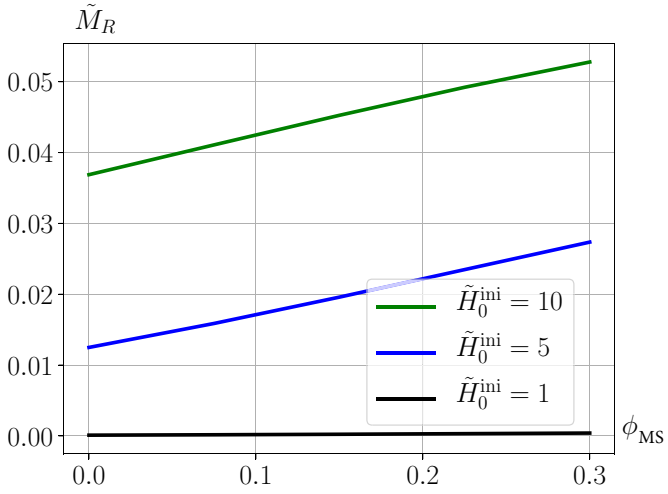

Figure 9. Dependence of remanent magnetisation of the MAE-MC model cell on the MS phase content for $\phi_{\mathrm{MH}} = 10\,\%$ and after initiating magnetisation by field $\tilde{H}_0^{\mathrm{ini}}$; the results are shown in dimensionless form.

a strong external field can by itself impart to the particles a sufficient remanent magnetisation, thus decreasing their magnetic permeability. Although the contribution of the MS phase to the internal field $\Delta H_{\mathrm{MH}} \propto \phi_{\mathrm{MS}}$ increases proportionally to ϕ_{MS}, its influence on $\tilde{M}_r$ in this field range is weak.

Once the initiating field is switched off, the MH particles magnetised to M_r polarise their MS environment. The total magnetic moment of the model cell is the sum of the magnetic moment $\boldsymbol{\mu}_{\mathrm{MH}}$ of the MH particle and the induced magnetic moment of the MS phase. At this point, the field and magnetisation distributions inside the cell are found by solving (12) under the condition $H_0 = 0$. As a result, the averaged remanent magnetisation of the model cell is determined by the expression

$$M_R = \frac{1}{V_{\Omega_2} + V_{\Omega_3}} \left[M_r V_{\Omega_2} + \int_{V_{\Omega_3}} \chi_{\mathrm{MS}}(H) H_z \, dV \right]. \qquad (15)$$

Figure 9 illustrates the most important result of the numerical calculations using the model cell, which is taken as a representative element of an MAE-MC. Evidently, the presence of the MS phase always enhances the macroscopic remanent magnetisation $\tilde{M}_R$. In other words, it is established that: *of the two competing contributions made by the MS phase to the remanent magnetisation of the cell, which are the closure of local magnetic fluxes (shielding) and the formation of local magnetic circuits between the MH particles, the latter one prevails.* The resulting increment of $\tilde{M}_R$ is but weakly pronounced for small initiating fields and low concentrations of the MS phase. However, it becomes significant with the increase of the initiating field, as shown by slopes of the lines in figure 9. For $\phi_{\mathrm{MS}} = 0.3$, the growth of $\tilde{M}_R$ is about 120% and 40% under fields $\tilde{H}_0^{\mathrm{ini}} = 5$ and 10, respectively. This strong effect stems definitely from the fact that for those field magnitudes, the remanent magnetisation of MH particles as a function of the applied field is rather steep, see figure 2. One could also predict qualitatively the tendency of the lines in figure 9 with further increase of the initiating field. For its higher values, the influence of the MS phase on $\tilde{M}_R$ would weaken, since MH particles cannot be magnetised beyond their saturation. As the field generated by each MH particle in the cell would approach a saturation field of the MS phase, the magnetisation $\tilde{M}_R$ would become virtually independent of ϕ_{MS}.

4. Experimental

For well-defined measurements of MAEs-MC, a special series of MAE-MC samples is prepared. All of them are moulded in the shape of identical prolate ellipsoids of revolution (spheroids) whose semiaxes are denoted as $c > a = b$, and the aspect ratio is fixed: $c/a = 3$, namely $a = 5$ mm and $c = 15$ mm.

The ingredients for the composite preparation are: a two-component silicone rubber Elastosil RT623 (Wacker Chemie AG, Germany) and two types of magnetic fillers. For the MH component, an NdFeB-alloy powder MQP-S-11-9-20 001-070 (Magnequench) [31] is used; this powder contains spherical particles with median diameter of 35–55 μm. The MS component consists of carbonyl iron powder (BASF, grade CC) [38]; the particles of this powder have spherical form and median diameter of 3.8–5.3 μm. Microscopic images of both types of powder are presented in figure 10.

The manufacturing process commences with mechanical mixing of the initially liquid rubber components with the prescribed amount of magnetic particles. The obtained dispersion is subjected to vacuuming inside an air compressor to eliminate air cavities prior to polymerisation. Then the prepared mixture is poured into a detachable casting aluminium mould. During the polymerisation process, which is carried out at room temperature, the filled mould is rotated on a loopster device at a rate of 10 rpm to prevent sedimentation of the metal micropowders.

Four samples with various magnetic content listed in table 1 are manufactured. Volume concentration of the MH filler in all samples has been maintained at a fixed value of 10 %; volume concentration of the MS phase is varied from 0 up to 30 %. The sample No. 1 is an MAE with only MH phase; samples Nos. 2–4 are MAEs-MC (figure 11).

Since all four samples contain the MH filler with high coercivity, they are initiated by a strong magnetic field $\boldsymbol{H}_{\mathrm{ext}}^{\mathrm{ini}}$. This is done in the electromagnet of Lake Shore 7407s magnetometer, where the samples are positioned in such a way that the longest (major) axis of the spheroids is parallel to the initiating field. Two different magnitudes of this field have been applied in turns to the samples. First, all samples of the set are magnetised with a field strength of $H_{\mathrm{ext}}^{\mathrm{ini}} = 637\,\mathrm{kA\ m^{-1}}$, and the field measurements around the samples are carried out as described below. After that, the spheroids are magnetised a second time in the same way, but with a field of $H_{\mathrm{ext}}^{\mathrm{ini}} = 1194\,\mathrm{kA\ m^{-1}}$, and the same set of measurements is repeated. If to express the magnitudes of the initiating field in the above introduced dimensionless form, they range 5 and 9.38, respectively. That is to say, two grades of the initial tuning (passive magnetic control) are applied in order to have the samples with different basic material properties.

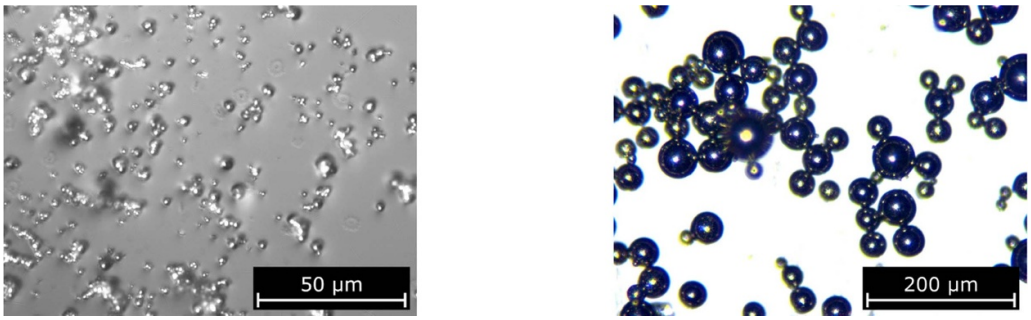

Figure 10. Microscopic images of MS powder (left: BASF, grade CC) and MH powder (right: Magnequench, MQP-S-11-9-20 001-070).

Table 1. Magnetic composition of the prolate spheroidal samples.

Sample No.	Type	ϕ_{MH}, vol%	ϕ_{MS}, vol%
1	MAE	10	0
2	MAE-MC	10	10
3	MAE-MC	10	20
4	MAE-MC	10	30

Figure 11. Synthesised prolate spheroidal samples initiated along their major axes.

By their size, the particles of both MH and MS powders are by orders of magnitude above the superparamagnetic limit and, therefore, expected to be highly magnetically stable. However, as the histograms of the commercial powders are quite wide, it could be possible that some portion of single-domain particles prone to superparamagnetism might be present and, thus, cause a magnetic ageing effect of the composites. To refute this presumption, the field measurements around the sample No. 4 are carried out two times: straight after its initiation by a field of 1194 kA m^{-1} and one year later. The difference between the measured field values is found to be less than 3%. This confirms that the magnetic ageing of the synthesised spheroids is negligible.

To evaluate the shear modulus of the composite matrix, unfilled samples in the form of rods of different lengths with a diameter of 4 mm are produced. The shear modulus is measured on a rotational rheometer (Anton Paar MCR301) using the quasi-statically torsional tests (SCF clamps), and it amounts to $G \approx 3.2$ MPa.

Each of the prepared spheroidal samples is fastened in the centre of a Helmholtz coil, whose axis of symmetry coincides with the longest axis of the spheroid. The spacial distribution of the magnetic field around the sample is scanned using a three-dimensional magnetic sensor (Infineon, TLV493D-A1B6). It is attached to a three-axis positioning system and can be moved along pre-programmed trajectories in a quasi-static regime with a given spatial pitch. Consider the cylindrical coordinate frame (ρ, θ, z) shown in figure 12. Due to the symmetry of the sample, the magnetic field along its principal $O\rho$ and Oz axes is directed in one direction along the Oz axis. The measurements of this field component are carried out under gradual increase of the distance between the magnetic sensor and the spheroid surface. The minimal distance from the surface is $d_{\min} = 0.65$ mm because of the actual dimensions of the sensor. For the minor $O\rho$ axis, the distance $d = \rho - a \geqslant d_{\min}$ is changed up to 5.65 mm in increments of 1 mm. For the major Oz axis, the distance $d = |z| - c \geqslant d_{\min}$ is increased gradually up to 10.65 mm with a step of 2 mm. In both cases, the measurements are accomplished in six points from two axially opposite sides, and the field values for each distance from the surface are averaged. The results are arranged in series with respect to spatial variables ρ and z, respectively.

As an active magnetic control to tune material properties of the first initiated samples, the magnetic field $\boldsymbol{H}_0$ of the Helmholtz coil is utilised. This external field is with high accuracy uniform in the region near the sample positioned at the coil centre, since the coil radius of 133 mm exceeds substantially the dimensions of the samples. The direction of the field is either parallel or opposed to the Oz axis, which is the direction of remanent magnetisation of the spheroid, see figure 12. Five moderate field strengths between –40 kA m^{-1} and 40 kA m^{-1} in increments of 20 kA m^{-1} are applied and for each of

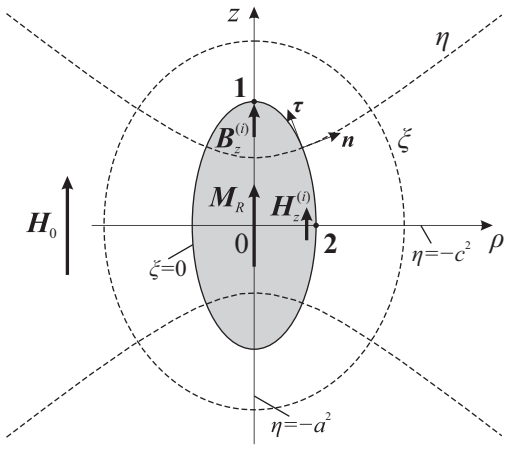

Figure 12. Prolate spheroid (grey) with a remanent magnetisation $\boldsymbol{M}_R$ in a uniform magnetic field $\boldsymbol{H}_0$ applied in the same direction. The uniform magnetic induction and field strength inside the spheroid are directed along the principal Oz axis and denoted by $\boldsymbol{B}_z^{(i)}$ and $\boldsymbol{H}_z^{(i)}$, respectively. The surfaces of constant prolate spheroidal coordinates (ξ,η) are shown by dashed lines.

them, the magnetic field measurements around the samples are conducted.

5. Magnetostatics of a macroscopic MAE-MC spheroid

The way of determining the material parameters—the remanent magnetisation and net magnetic susceptibility—of the MAEs-MC from the data of spatial scanning of the magnetic field z-component outside along the axes of the spheroidal samples, follows from the macroscopic magnetostatics.

5.1. Magnetised spheroid in a uniform field

Consider a prolate spheroid with semiaxes $c>a=b$, along whose the longest axis is the Oz axis of a cylindrical coordinate system (ρ,θ,z), see figure 12. Assume that the spheroid possesses a spatially uniform remanent magnetisation $\boldsymbol{M}_R$ directed along Oz, and a uniform magnetic (probing) field $\boldsymbol{H}_0$ is imposed in the same direction. As the sample is a spheroid, both the magnetic induction and field strength inside of it are uniform and parallel to the applied field; note that this assumption has already been used successfully in the problem of bending vibrations of the MAE cantilevers comprising MS particles [39]. In addition, the polymer matrix of the material is taken to be rigid enough (Young modulus $E=3G\sim 10^7$ Pa, see section 4), so that the striction strain induced by a magnetic field may be neglected.

The problem of the magnetic field distribution is described by (8) and is solved in prolate spheroidal coordinates (ξ,η). The surfaces of constant ξ and η are prolate spheroids and hyperboloids of revolution of two sheets (figure 12). The sought magnetostatic potentials $\psi^{(i)}(\xi,\eta)$ and $\psi^{(e)}(\xi,\eta)$ introduced by (9) inside and outside the spheroid, respectively, are well known [36, 40]. Deriving the magnetic induction, one finds that the induction $\boldsymbol{B}^{(i)}$ inside the spheroid has only one non-zero component:

$$\frac{1}{\mu_0}B_z^{(i)}=\frac{(1+\chi)H_0+(1-\mathcal{N}_z)M_R}{1+\chi\mathcal{N}_z}, \tag{16}$$

where χ is the macroscopic net magnetic susceptibility of the material of which the spheroid is made, and $\mathcal{N}_z$ the demagnetising coefficient along the Oz axis of the spheroid. For tested spheroids with a semiaxes ratio $c/a=3$, this coefficient equals to $\mathcal{N}_z\simeq 0.11$ [41]. The magnetic field strength inside the spheroid is $H_z^{(i)}=(H_0-\mathcal{N}_zM_R)\,(1+\chi\mathcal{N}_z)^{-1}$, and it is reduced in comparison with the applied field H_0 due to the demagnetising correction and remanence.

The general formula for the magnetic induction $\boldsymbol{B}^{(e)}$ outside the spheroid is too cumbersome to be written in full. Instead, we present only two particular expressions, those along the two principal axes of the coordinate frame:

$$\frac{1}{\mu_0}B_z^{(e)}\,(\rho=0,z)\approx H_0+\frac{2a^2c}{3z^3}\,\frac{\chi H_0+M_R}{1+\chi\mathcal{N}_z}+\mathcal{O}(z^{-5}), \tag{17}$$

$$\frac{1}{\mu_0}B_z^{(e)}\,(\rho,z=0)\approx H_0-\frac{a^2c}{3(\rho^2-a^2+c^2)^{3/2}}\,\frac{\chi H_0+M_R}{1+\chi\mathcal{N}_z}+\mathcal{O}(\rho^{-5}). \tag{18}$$

Both of them retain sufficient accuracy down to the very surface of the spheroid. Note that here H_0 denotes a probing field that is much lower than the initiating one $H_{\rm ext}^{\rm ini}$.

5.2. Interpretation of the measurement data

Formulas (17) and (18) suffice to extract from the field measurement data the main macroscopic magnetic parameters of the sample, viz. its susceptibility χ and remanence M_R.

Consider two particular points 1 and 2 on the surface of the spheroid as shown in figure 12. Evidently, due to the finite dimensions of a magnetic field sensor, it is impossible to measure the field values precisely at these points. However, we assume that the measurements along the axes are described approximately by expressions (17) and (18) right up to the surface.

From the boundary conditions in (8), it follows that at point 1 the normal, that along the Oz axis, component of magnetic induction is continuous across the boundary: $B_{z1}^{(e)}=B_z^{(i)}$ where the latter is given by (16). At point 2 (i.e. at $\rho=a$ and $z=0$), the magnetic field strength is tangential to the sample surface, it points along Oz and is continuous as well. Hence, one has $B_{z2}^{(e)}=\mu_0H_{z2}^{(e)}=\mu_0H_z^{(i)}$, where the latter value is already defined, see the text below (16).

For further use, it is convenient to introduce the difference of the reference field values as a function of the probing field $\boldsymbol{H}_0$:

$$\Delta_{H_0}=\frac{1}{\mu_0}\left(B_{z1}^{(e)}-B_{z2}^{(e)}\right)=\frac{\chi H_0+M_R}{1+\chi\mathcal{N}_z}. \tag{19}$$

In the basic state, i.e. in the absence of an external field $H_0=0$, the field difference (19) establishes a linear relation

Table 2. Macroscopic material parameters M_R and χ of the spheroidal samples magnetised in two different initiating fields: mean value $\pm$ standard deviation of four measurements taken on each side along the principal axes of the spheroid.

		$H_{\text{ext}}^{\text{ini}} = 637\,\text{kA m}^{-1}$		$H_{\text{ext}}^{\text{ini}} = 1194\,\text{kA m}^{-1}$	
Sample No.	Type	M_R, kA m^{-1}	χ	M_R, kA m^{-1}	χ
1	MAE	17.92 ± 2.48	0.036 ± 0.096	57.73 ± 3.26	0.041 ± 0.018
2	MAE-MC	23.98 ± 2.49	0.553 ± 0.106	66.47 ± 4.82	0.599 ± 0.052
3	MAE-MC	32.37 ± 3.18	1.405 ± 0.045	75.92 ± 5.22	1.360 ± 0.131
4	MAE-MC	37.03 ± 2.62	2.331 ± 0.062	80.70 ± 3.41	2.405 ± 0.158

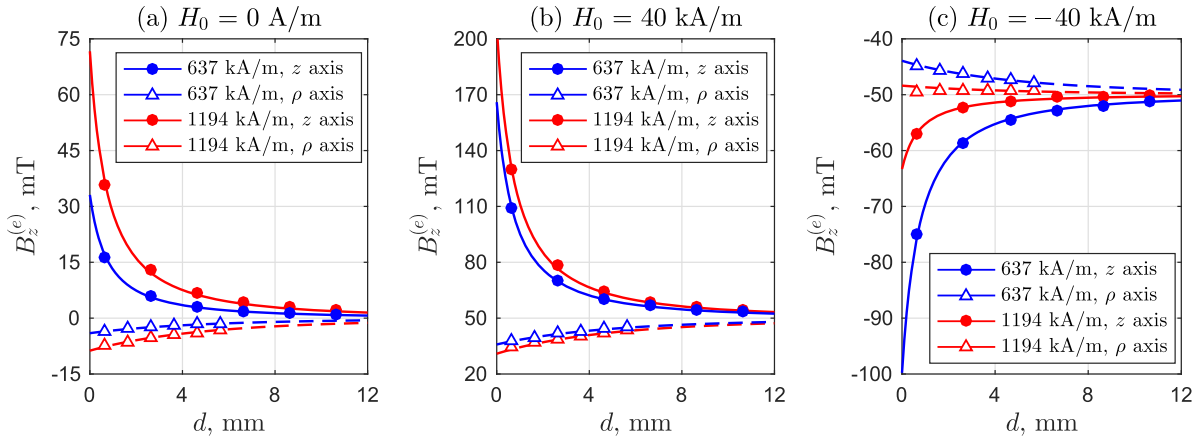

Figure 13. Magnetic induction $B_z^{(e)}$ near the magnetised MAE-MC spheroid No. 4 as a function of the distances $d = \rho - a$ and $d = z - c$ from its surface along the major $O\rho$ and Oz axes, respectively, under a uniform external field H_0 of: (a) 0 A m^{-1}; (b) 40 kA m^{-1}; (c) -40 kA m^{-1}. Experimental measurements are shown by markers. Theoretical calculations based on (17) and (18) are shown as lines for $H_{\text{ext}}^{\text{ini}} = 637$ kA m^{-1} (blue): $\chi = 2.331$ and $M_R = 37.03$ kA m^{-1}; for $H_{\text{ext}}^{\text{ini}} = 1194$ kA m^{-1} (red): $\chi = 2.405$ and $M_R = 80.7$ kA m^{-1}.

between the remanent magnetisation and the macroscopic susceptibility of the sample material: $M_R = \Delta_0\,(1 + \chi\mathcal{N}_z)$. If the same measurements are carried out under a moderate probing field $\boldsymbol{H}_0 \parallel Oz$, then substitution of the above-defined M_R in (19) provides the explicit expression for the macroscopic susceptibility of the MAE-MC in terms of experimentally measured quantities:

$$\chi = \frac{\Delta_{H_0} - \Delta_0}{H_0 - \mathcal{N}_z\,(\Delta_{H_0} - \Delta_0)}. \tag{20}$$

The remanent magnetisation writes in the same terms as

$$M_R = \frac{H_0\,\Delta_0}{H_0 - \mathcal{N}_z\,(\Delta_{H_0} - \Delta_0)}. \tag{21}$$

We note that (20) and (21) may be presented in yet another form. Indeed, it is evident that under a moderate probing field the difference $\Delta_{H_0} - \Delta_0$ should be linear in the strength H_0, so that this dependence may be characterised by a coefficient $K \equiv (\Delta_{H_0} - \Delta_0)/H_0$. Given that (20) and (21) transform to

$$\chi = K/\,(1 - K\mathcal{N}_z), \quad M_R = \chi\Delta_0/K. \tag{22}$$

Therefore, the presented expressions define the procedure of evaluating the main magnetic material parameters of an MAE-MC from the magnetic measurements outside of a spheroidal sample.

The 'building blocks' for Δ_0 and Δ_{H_0}, i.e. the field values $B_{z1}^{(e)}$ and $B_{z2}^{(e)}$ on the surface of the spheroid, are not directly measurable due to the finite size of the magnetic sensor. To get them, we use the coordinate dependencies (17) and (18) substituting there the minimal distance $d_{\min} = 0.65$ mm of the sensor. Therefore, this gives

$$\begin{aligned}\Delta_{H_0}(d_{\min}) = \frac{1}{\mu_0}\Big(&B_z^{(e)}\,(\rho = 0, z = c + d_{\min}) \\ &- B_z^{(e)}\,(\rho = a + d_{\min}, z = 0)\Big) \\ &\approx 0.55 \cdot \frac{\chi H_0 + M_R}{1 + \chi\mathcal{N}_z},\end{aligned} \tag{23}$$

which refers to the field-dependent experimental dependencies of Δ_{H_0}. After that, the macroscopic characteristics of the MAEs-MC spheroids with different volume content of the MS phase and initiated by different fields are obtained. In each case, the parameter set (M_R, χ) is evaluated with the use of formulas (20) and (21) by considering four measurements of the field taken on each side along the principal $O\rho$ and Oz axes of the spheroid. These results are presented in table 2.

As an illustration, for the MAE-MC spheroid No. 4 with $\phi_{\text{MH}} = 10\,\%$ and $\phi_{\text{MS}} = 30\,\%$, figure 13 shows the experimental and theoretical coordinate dependencies of the magnetic induction component $B_z^{(e)}$ in case of three different probing fields H_0. Theoretical dependencies are calculated using the corresponding material parameters from table 2 by means of relations (17) and (18).

Figure 14 presents verification results for all four samples. As can be seen, the experimentally found dependence of the

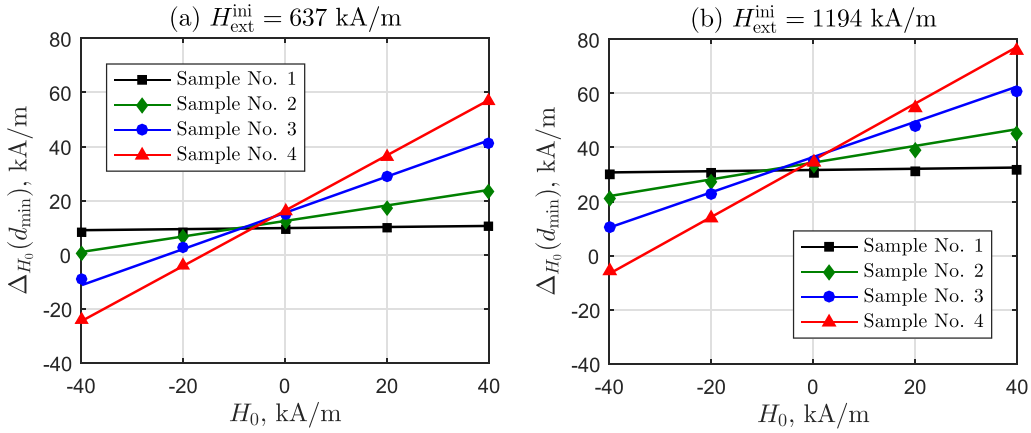

Figure 14. Field difference $\Delta_{H_0}(d_{\rm min})$ between the magnetic induction components close to the tip (point 1) and to the 'equator' (point 2) of a spheroid at a distance $d_{\rm min} = 0.65$ mm from its surface; the initiating fields $H_{\rm ext}^{\rm ini}$ are: (a) 637 kA m^{-1}; (b) 1194 kA m^{-1}. Experimental measurements are shown by markers. The lines show the theoretical dependence given by (23) calculated for the mean values of the evaluated material parameters χ and M_R presented in table 2.

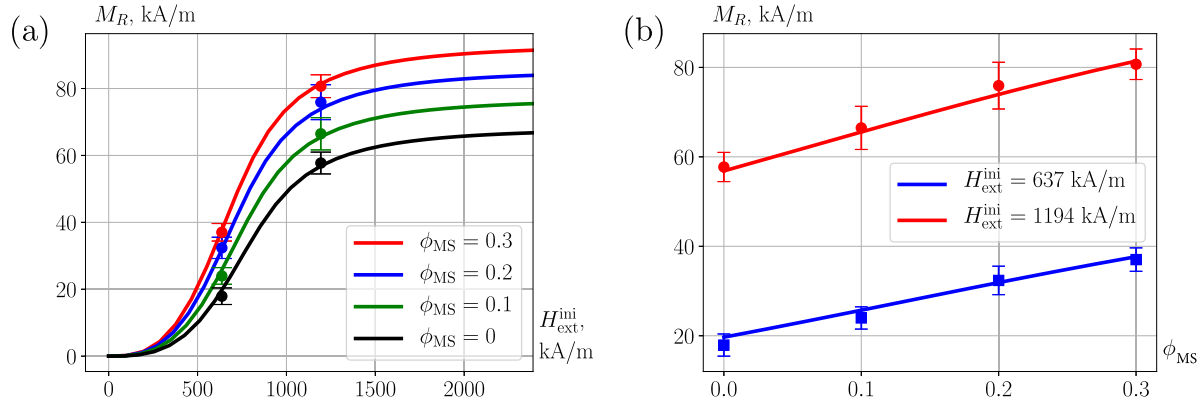

Figure 15. Remanent magnetisation M_R of MAEs-MC with a fixed volume amount of the MH phase $\phi_{\rm MH} = 10$ % dependent on (a) the initiating field $H_{\rm ext}^{\rm ini}$ and (b) the volume concentration $\phi_{\rm MS}$ of the MS phase ranging from 0 to 30 %. Markers show the experimental measurement results for the samples initiated with $H_{\rm ext}^{\rm ini} = 637$ kA m^{-1} and 1194 kA m^{-1} (table 2). Theoretical calculations using the model cell with the same volume contents are shown as lines for the parameter values given by (14).

parameter $\Delta_{H_0}(d_{\rm min})$ on the probing field H_0 obeys the theoretically predicted linear dependence (23).

6. Concentration dependence of the magnetic parameters of MAE-MC: Mesoscopic interpretation

The evaluated macroscopic material parameters χ and M_R of the tested MAEs-MC (table 2) depend notably on the concentration of the MS phase. These dependencies are essential for predicting field-tuning magnetomechanical properties of MAEs-MC during active magnetic control. The origin of the concentration effect evidently cannot be analysed in the framework of a macroscopic (phenomenological) approach. Hereby we apply for that purpose the mesoscopic model developed in sections 2 and 3.

As a first step, the net magnetisation $M^{\rm ini}(H_0^{\rm ini}, \phi_{\rm MS})$ of the composite at the initiation is calculated numerically. This enables using relation (1) to transform the initiating field $H_{\rm ext}^{\rm ini}$ of the laboratory solenoid into the field $H_0^{\rm ini}$ acting inside the spheroidal sample with a given demagnetising factor.

To calibrate the theory, i.e. to evaluate the adjustable parameter H_*, the function (4) is adjusted using (1) to the obtained experimental data of M_R for the case of $\phi_{\rm MS} = 0$ (sample No. 1 in table 2). To a good extent, this procedure is described in section 3, and for the considered case, the values of material parameters are given in set (14). In particular, we recover a value of $H_* = 547.5$ kA m^{-1}. The resulting curve is shown in figure 7, and it is the lowest one in figure 15(a). As can be seen, the proposed approximation complies well with the measurement data, albeit these data are rather scarce.

Magnetisation curves of the MAEs-MC samples, which contain up to 30 % of the MS phase, in figure 15(a) are calculated along the procedure described in section 3.3. For the MS phase, the Fröhlich–Kennelly law (6) is used, whereas the concentration dependence of the susceptibility $\chi_{\rm MS}^0$ is taken in the Lichtenecker form (7) and the saturation magnetisation $M_{\rm MS}^{\rm (sat)}$ grows linearly with increasing $\phi_{\rm MS}$. For every value of $\phi_{\rm MS}$, the problem of initiating magnetisation is solved anew, and from its solution, the function $H_{\rm MH}^{\rm ini}(H_{\rm ext}^{\rm ini})$ is evaluated by (13). This dependence is then used in (3) to obtain the remanent

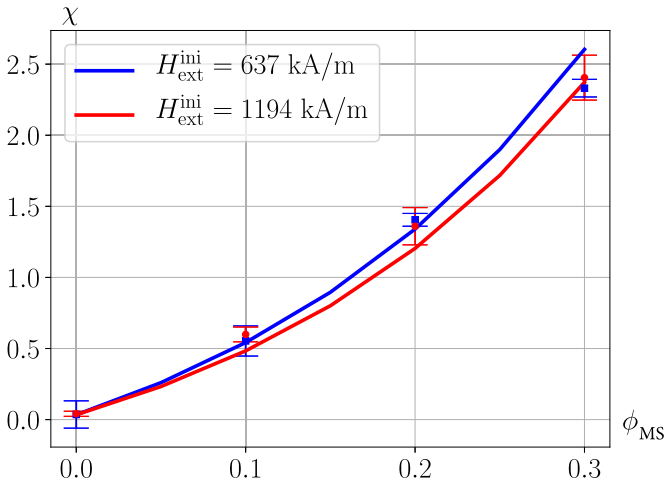

Figure 16. Macroscopic susceptibility χ of MAEs-MC with a fixed volume amount of the MH phase $\phi_{MH} = 10\,\%$ dependent on the volume MS content ϕ_{MS} ranging from 0 to 30 % for the initiating fields $H_{ext}^{ini} = 637\,\mathrm{kA\,m^{-1}}$ (blue) and $1194\,\mathrm{kA\,m^{-1}}$ (red). Markers show the experimental measurement results (table 2). Theoretical calculations using the model cell with the same volume contents are shown as lines for the parameter values given by (14).

magnetisation $M_r(H_{MH}^{ini}, H_*)$ of the MH particles, since in this situation it depends on the volume content of the MS phase. With the obtained magnetisation of the MH particles, the net remanent magnetisation M_R of the cell is determined with the aid of relation (15). The results of comparison with the experimental data from table 2 are presented in figure 15(b), and the achieved agreement is fairly good.

In the framework of the model, evaluation of the net susceptibility of the cell, which is associated with the susceptibility χ of an MAE-MC obtained from the field measurements, is done on the same basis. Comparison of the results for the model cell with the experimental data from table 2 is presented in figure 16. As it is seen, the predicted non-linearity of $\chi(\phi_{MS})$ describes the experiment quite well in all the concentration range investigated. The deviation between the theoretical curves at higher concentrations reflects the fact that the stronger the field generated by the MH particles is, the closer the MS fraction is to saturation and, thus, responds with lower susceptibility. On the other hand, figure 16 evidences that despite the almost two-times difference in initiating fields, the occurring discrepancy between the susceptibilities of the samples is not large; this fact follows directly from the data of table 2 as well.

7. Conclusions

Magnetic properties of MAEs-MC pose a complicated problem for analysing due to several circumstances. One of them, being seemingly just technical, entails important consequences. Its key factor is that the initiating process is carried out with the laboratory setups, which are unable to produce an initiating field H_{ext}^{ini} that is sufficiently strong to saturate fully contained MH particles. On the one hand, the field H_{ext}^{ini} of the order of 800–1600 kA m^{-1}, once applied and then turned off, brings the remanence M_r of MH particles to a level that ensures notable remanence M_R of the entire MAE-MC sample. On the other hand, the field H_{ext}^{ini} of such an order comes to a limit attainable in laboratory yet in the range where the rate dM_r/dH_{ext}^{ini} is still rather high. Under the condition that the function $M_r\left(H_{ext}^{ini}\right)$ retains considerable steepness, any, even rather moderate, bias field ΔH of 80–160 kA m^{-1} that adds to H_{ext}^{ini} is able to change strongly the resulting remanence $M_r(H_{ext}^{ini} + \Delta H)$. When the MS phase, e.g. carbonyl iron micropowder, is present in the sample, it becomes readily a source of such a bias field, since it saturates at fields much weaker than that used for the initiation. This effect is the greater the higher the volume content of the MS phase. Evidently, to describe it, one has to take into account the magnetic interaction between the phases; note that it exists in MAEs-MC independently of the absence/presence of external field.

This effect is, in fact, just a particular manifestation of a more universal feature of the magnetic interaction inherent to MAEs-MC that does depend on the actual strength of H_{ext}^{ini}. When the initiating field is on, (*i*) the MS phase distributed around MH particles screens the external field working on each MH particle, whereas (*ii*) MS particles residing in the gap between MH particles work as magnetic bridges, which enhance this acting field. The same twofold interaction effect occurs in the basic state, when H_{ext}^{ini} is turned off: the MS phase favors partially the magnetic flux closure around each MH particle, but between adjoining MH particles it forms a magnetic circuit. The interplay of those contributions to the macroscopic magnetisation defines the resulting remanence M_R of the MAE-MC.

The proposed modelling of an MAE-MC using the mesoscopic model cell is constructed to account for the above-described duality of the MH–MS magnetic interactions. Despite its simplified mesostructure, the model cell proves to deliver both a full qualitative and a fairly good quantitative description of the concentration dependence of the basic magnetic characteristics, such as the net susceptibility and remanent magnetisation, of the synthesised MAEs-MC with various composition.

Acknowledgment

Financial support of the research association PAK907 between the Deutsche Forschungsgemeinschaft (DFG) and the Russian Foundation for Basic Research (RFBR) under the projects # 19-52-12045, BE-6553/1-1, ZI 540-17/3 and BO 3343/2-1 within SPP1681 and PAK907 is gratefully acknowledged. We would like to thank Joseph Beerel, a student at the Technische Universität Ilmenau, for carrying out the magnetic field measurements around the spheroidal samples.

ORCID iDs

T I Becker https://orcid.org/0000-0003-2473-1599
D Yu Borin https://orcid.org/0000-0003-3842-1487
Yu L Raikher https://orcid.org/0000-0002-6167-6528

References

[1] Rigbi Z and Jilkén L 1983 The response of an elastomer filled with soft ferrite to mechanical and magnetic influences *J. Magn. Magn. Mater.* **37** 267–76

[2] Jolly M R, Carlson J D and Munoz B C 1996 The magnetoviscoelastic response of elastomer composites consisting of ferrous particles embedded in a polymer matrix *J. Intell. Mater. Syst. Struct.* **7** 613–22

[3] Nikitin L V, Mironova L S, Stepanov G V and Samus A N 2001 The influence of a magnetic field on the elastic and viscous properties of magnetoelastics *Polymer Sci.* A **43** 443–50

[4] Varga Z, Filipcsei G and Zrínyi M 2006 Magnetic field sensitive functional elastomers with tuneable elastic modulus *Polymer* **47** 227–33

[5] Nikitin L V, Stepanov G V, Mironova L S and Gorbunov A I 2004 Magnetodeformational effect and effect of shape memory in magnetoelastics *J. Magn. Magn. Mater.* **272–276** 2072–3

[6] Stepanov G V, Borin D Yu, Raikher Yu L, Melenev P V and Perov N S 2008 Motion of ferroparticles inside the polymeric matrix in magnetoactive elastomers *J. Phys.: Condens. Matter.* **20** 204121

[7] Stolbov O V, Raikher and Balasoiu M 2011 Modelling of magnetodipolar striction in soft magnetic elastomers *Soft Matter* **7** 8484–7

[8] Gundermann T and Odenbach S 2014 Investigation of the motion of particles in magnetorheological elastomers by X-μCT *Smart Mater. Struct.* **23** 105013

[9] Li Y, Li J, Li W and Du. H 2014 A state-of-the-art review on magnetorheological elastomer devices *Smart Mater. Struct.* **23** 123001

[10] Odenbach S 2016 Microstructure and rheology of magnetic hybrid materials *Arch. Appl. Mech.* **86** 269–79

[11] Volkova T I, Böhm V, Kaufhold T, Popp J, Becker F, Borin D Y, Stepanov G V and Zimmermann K 2017 Motion behaviour of magneto-sensitive elastomers controlled by an external magnetic field for sensor applications *J. Magn. Magn. Mater.* **431** 262–5

[12] Dobrzánski L A and Drak M 2004 Structure and properties of composite materials with polymer matrix reinforced Nd-Fe-B hard magnetic nanostructured particles *J. Mater. Process. Technol.* **157–158** 650–7

[13] Makled M H, Matsui T, Tsuda H, Mabuchi H, El-Mansy M K and Morii K 2005 Magnetic and dynamic mechanical properties of barium ferrite–natural rubber composites *J. Mater. Process. Technol.* **160** 229–33

[14] von Lockette P R, Lofland S E, Biggs J, Roche J, Mineroff J and Babcock M 2011 Investigating new symmetry classes in magnetorheological elastomers: cantilever bending behavior *Smart Mater. Struct.* **20** 10502

[15] Stepanov G V, Chertovich A V and Kramarenko E Yu 2012 Magnetorheological and deformation properties of magnetically controlled elastomers with hard magnetic filler *J. Magn. Magn. Mater.* **324** 3448–51

[16] Sheridan R, Roche J, Lofland S E and von Lockette P R 2011 Numerical simulation and experimental validation of the large deformation bending and folding behavior of magneto-active elastomer composites *Smart Mater. Struct.* **20** 10502

[17] Anderson K, Bravoco R, Hargrave W, von Lockette P R and Lofland S E 2015 Dynamic shear response of hard versus soft magnetic magnetoactive elastomers *Smart Mater. Struct.* **20** 025022

[18] Kramarenko E Yu, Chertovich A V, Stepanov G V, Semisalova A S, Makarova L A, Perov N S and Khokhlov A R 2015 Magnetic and viscoelastic response of elastomers with hard magnetic filler *Smart Mater. Struct.* **24** 035002

[19] Stepanov G V, Borin D Y and Storozhenko P A 2017 Rotation of magnetic particles inside the polymer matrix of magnetoactive elastomers with a hard magnetic filler *J. Magn. Magn. Mater.* **431** 138–40

[20] Zhao R, Kim Y, Chester S A, Sharma P and Zhao X 2019 Mechanics of hard-magnetic soft materials *J. Mech. Phys. Solids* **124** 244–63

[21] Breznak C and von Lockette P R 2019 Particle orientation and bulk properties of magnetoactive elastomers fabricated with aligned barium hexaferrite *J. Mater. Res.* **34** 972–81

[22] Borin D Y, Stepanov G V and Odenbach S 2013 Tuning the tensile modulus of magnetorheological elastomers with magnetically hard powder *J. Phys. Conf. Ser.* **412** 012040

[23] Borin D Y and Stepanov G V 2013 Oscillation measurements on magnetoactive elastomers with complex composition *J. Optoelectron. Adv. Mater.* **15** 249–53

[24] Stepanov G V, Borin D Y, Bakhtiiarov A V and Storozhenko P A 2017 Magnetic properties of hybrid elastomers with magnetically hard fillers: rotation of particles *Smart Mater. Struct.* **26** 035060

[25] Borin D Y, Stepanov G V and Odenbach S 2019 Stress induced by the striction of hybrid magnetoactive elastic composites *J. Magn. Magn. Mater.* **470** 85–9

[26] Borin D Y, Stepanov G and Dohmen E 2019 Hybrid magnetoactive elastomer with a soft matrix and mixed powder *Arch. Appl. Mech.* **89** 105–17

[27] Linke J M, Borin D Y and Odenbach S 2016 First-order reversal curve analysis of magnetoactive elastomers *RSC Adv.* **6** 100407–16

[28] Biller A M and Stolbov O V and Raikher Y L 2015 Mesoscopic magnetomechanical hysteresis in a magnetorheological elastomer *Phys. Rev.* E **92** 023202

[29] Cremer P, Löwen H and Menzel A M 2016 Superelastic stress–strain behavior in ferrogels with different types of magneto-elastic coupling *Phys. Chem. Chem. Phys.* **18** 26670–90

[30] Puljiz M, Huang S, Kalina K A, Nowak J, Odenbach S, Kästner M, Auernhammer G K and Menzel A M 2018 Reversible magnetomechanical collapse: virtual touching and detachment of rigid inclusions in a soft elastic matrix *Soft Matter* **14** 6809–21

[31] Magnequench 2009 *MQP-S-11-9-20001-070 isotropic powder* Material description

[32] Coey J M D 2010 *Magnetism and Magnetic Materials* (Cambridge: Cambridge University Press)

[33] Stoner E C and Wohlfarth E P 1948 A mechanism of magnetic hysteresis in heterogeneous alloys *Phil. Trans. R. Soc.* A **240** 599–642

[34] Bozorth R M 1993 *Ferromagnetism* (New York, Piscataway, NJ: Wiley-IEEE Press)

[35] Zakri T, Laurent J-P and Vauclin M 1998 Theoretical evidence for Lichtenecker's mixture formulae based on the effective medium theory *J. Phys. D: Appl. Phys.* **31** 1589–94

[36] Landau L D, Lifshitz E M and Pitaevskii L P 1984 *Electrodynamics of Continuous Media* (Oxford: Pergamon)

[37] www.fenicsproject.org.

[38] (https://www.dispersions-pigments.basf.com/portal/load/fid827906/CIP_General_PO_e.pdf)

[39] Becker T I, Raikher Y, Stolbov O, Böhm V and Zimmermann K 2017 Dynamic properties of magneto-sensitive elastomer cantilevers as adaptive sensor elements *Smart Mater. Struct.* **26** 095035

[40] Jackson J D 1962 *Classical Electrodynamics* (New York: Wiley)

[41] Osborn J A 1945 Demagnetizing factors of the general ellipsoid *Phys. Rev.* **67** 351–7